



HAL
open science

Rare earth oxide promoted Ru/Al₂O₃ dual function materials for CO₂ capture and methanation: An operando DRIFTS and TGA study

Lizbeth Moreno Bravo, F. Meunier, Jan Kopyscinski

► To cite this version:

Lizbeth Moreno Bravo, F. Meunier, Jan Kopyscinski. Rare earth oxide promoted Ru/Al₂O₃ dual function materials for CO₂ capture and methanation: An operando DRIFTS and TGA study. *Applied Catalysis B: Environmental*, 2025, 361, pp.124591. 10.1016/j.apcatb.2024.124591 . hal-04713859

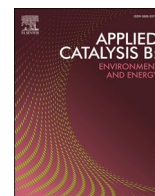
HAL Id: hal-04713859

<https://hal.science/hal-04713859v1>

Submitted on 9 Oct 2024

HAL is a multi-disciplinary open access archive for the deposit and dissemination of scientific research documents, whether they are published or not. The documents may come from teaching and research institutions in France or abroad, or from public or private research centers.

L'archive ouverte pluridisciplinaire **HAL**, est destinée au dépôt et à la diffusion de documents scientifiques de niveau recherche, publiés ou non, émanant des établissements d'enseignement et de recherche français ou étrangers, des laboratoires publics ou privés.



Rare earth oxide promoted Ru/Al₂O₃ dual function materials for CO₂ capture and methanation: An *operando* DRIFTS and TGA study

Lizbeth Moreno Bravo^a, Frederic C. Meunier^{b,*}, Jan Kopyscinski^{a,*}

^a Department of Chemical Engineering, McGill University, 3610 University Street, Montreal, Canada

^b Institut de Recherche sur la Catalyse et l'Environnement de Lyon, 2 Av. Albert Einstein, Villeurbanne 69626, France

ARTICLE INFO

Keywords:

CO₂ capture
CO₂ methanation
Operando DRIFTS
DFMs
Rare earth oxides

ABSTRACT

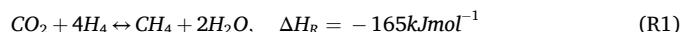
Dual-function materials (DFMs) combine sorbent and catalytic components to perform selective CO₂ capture and subsequent hydrogenation. This study explores the performance of rare-earth oxides (REOs) as CO₂ adsorption sites on Ru/Al₂O₃. REOs increase CO₂ uptake by upwards of +60 % by enhancing the overall catalyst surface basicity and favoring metal-support interactions. Thermogravimetric analysis during CO₂ adsorption-hydrogenation cycles exhibited significant catalytic activity and enhanced stability of Ru-REO/Al₂O₃ at temperatures as low as 200 °C. This leads to methane production of 50–85 μmol g⁻¹, surpassing recently reported values obtained for alkali and alkali-earth promoted Ru-based materials operated at 250 °C. The highest performing studied DFM, RuNd₂O₃/Al₂O₃, achieved 85 % CO₂ capture efficiency and steadily produced methane in cyclic operation (+120 % CO₂ uptake relative to Ru/Al₂O₃). *Operando* DRIFTS revealed that the dominant mechanism for methane formation is the hydrogenation of ruthenium carbonyls, which are stabilized by REOs. Upon CO₂ exposure, surface carbonates and bicarbonate species form more abundantly on DFMs than on Ru/Al₂O₃. This confirms that REOs enhance the adsorption and retention of carbonates, which generate additional promoter-related reaction pathways during low-temperature hydrogenation. These findings are crucial in the advancement of sustainable, wider operation range carbon capture and utilization technologies.

1. Introduction

In developing a carbon-neutral energy sector, an increased market penetration of cheaper renewable energy necessitates the development of robust and scalable energy storage on varied timescales. Carbon capture and utilization (CCU) technologies are of significant interest in long-term storage solutions due to their net positive effect on the global carbon balance and their adaptability to the existing industrial storage and transport infrastructure [1]. Power-to-gas (PtG) processes bridge renewable energy production to long-term storage through the production of H₂ via water electrolysis (green H₂). To couple this with CCU processes, captured CO₂ can be used as feedstock to react with green H₂ to obtain grid-compatible gas (methane) or other hydrocarbons [2]. Methane produced through this route, referred to as renewable natural gas (RNG), can be mixed with extracted methane and used in numerous areas such as transportation, industrial processes, heating, and the production of chemicals [3].

In recent years, research has focused on combining CO₂ capture and its subsequent methanation within the same reactor by using dual-

function materials (DFMs) [4–7]. DFMs contain both sorbent and catalytic components, enabling selective CO₂ capture from a gas stream before hydrogenation to CH₄ via cyclic operations at a constant temperature. The main reaction of the Sabatier process is CO₂ methanation (R1),



DFMs ideally demonstrate good regeneration ability, high conversion rate, and selectivity like typical catalysts. To enable both functions, their design requires consideration of generating adsorption and reactive sites. In the Sabatier process, DFMs require one site type for CO₂ adsorption, typically an alkali or alkaline-earth metal oxide (CaO, Na₂O, MgO, etc.) and a neighboring catalytic site that enables CO₂ hydrogenation, commonly a transition metal (Ru, Rh, Pt, Ni) [4,5,8,9]. These metals and oxides are usually supported on materials with large surface areas (80–200 m² g⁻¹), such as Al₂O₃ [4]. Loadings of 1–10 wt % for sorbents and metals have been investigated with a reported total CO₂ storage capacity of up to 19 g_{CO2} kg_{DFM}⁻¹ (~425 mmol_{CO2} kg_{DFM}⁻¹) [4, 5].

* Corresponding authors.

E-mail addresses: fcm@ircelyon.univ-lyon1.fr (F.C. Meunier), jan.kopyscinski@mail.mcgill.ca (J. Kopyscinski).

<https://doi.org/10.1016/j.apcatb.2024.124591>

Received 17 May 2024; Received in revised form 4 September 2024; Accepted 9 September 2024

Available online 10 September 2024

0926-3373/© 2024 The Author(s). Published by Elsevier B.V. This is an open access article under the CC BY-NC-ND license (<http://creativecommons.org/licenses/by-nc-nd/4.0/>).

To further enhance the efficacy of DFMs in the capture and utilization of carbon dioxide, we propose the novel application of rare-earth oxides (REOs) as adsorption sites on ruthenium-alumina catalysts. Exhibiting similar catalytic behavior to that of alkaline-earth oxides, REOs influence the material's relative basicity, surface structure, and CO₂ uptake due to their distinctive solid-state characteristics [10].

REOs have been investigated as supports or catalyst additives for similar, continuous reaction systems. The incorporation of CeO₂ to Ni/Al₂O₃ catalysts has been proven to increase conversion up to 20 % in dry reforming of methane (DRM) reactions, while reducing carbon deposition compared to non-modified catalysts [11,12]. The electronic structure and lattice properties of REOs translate into diverse acid-base traits, notable redox activity, and high oxygen storage capacity, which can improve catalyst stability, resistance to coking, and pore sintering [13–15].

Research studies on Gd₂O₃-modified Ni/Al₂O₃ catalysts showed that overall CO₂ adsorption capacity was augmented, and CH₄ yield for CO₂ methanation at 200–250 °C was higher for Gd₂O₃-modified catalysts compared to unmodified Ni/Al₂O₃. These improvements are attributed to greater metal dispersion, enabled by REOs, which increases the surface area for reaction [16]. Similarly, work from Namvar *et al.* [17] found that Nd-modified Ni/Al₂O₃ catalysts exhibited a 15 % higher CO₂ conversion rate than unmodified Ni/Al₂O₃ catalysts at 350 °C methanation.

REOs strengthen metal-support interactions by altering the electronic environment of the surrounding catalytic metal sites and generating oxygen vacancies [18–20]. The versatile nature of REOs in addition to their ability to create additional active sites for CO₂ adsorption and hydrogenation, makes them ideal candidates for their use in DFM systems. In this work, we integrate REOs into DFMs by introducing CeO₂, Gd₂O₃, Sm₂O₃, and Nd₂O₃ into Ru/Al₂O₃ catalysts to produce DFMs, which enhance both CO₂ capture and methanation catalytic activity at low temperatures (200 °C), widening the operating range of DFM systems. The materials' performances as DFMs are evaluated using thermogravimetric analyses (TGA) and *operando* diffuse reflectance infrared Fourier Transform spectroscopy (DRIFTS) studies and are compared to a traditional 5 wt% Ru/Al₂O₃ catalyst and 10 wt% REO/Al₂O₃ materials. To better understand the REOs role during the Sabatier process, reaction intermediate species are identified, and potential reaction pathways are discussed in view of future advances in DFM development.

2. Experimental

2.1. Catalyst preparation

Catalysts were prepared using successive incipient wetness impregnation. First, alumina (Al₂O₃, Alfa-Aesar) was ground and sieved to ensure a particle size of 90 – 125 μm. Samples containing rare-earth metals were impregnated for 14 h by an aqueous solution of their corresponding nitrate precursors (Gd(NO₃)₃·6 H₂O, ≥ 99.9 %, Sigma Aldrich; Sm(NO₃)₃·6 H₂O, ≥ 99.9 %, Fisher Scientific; Nd(NO₃)₃·6 H₂O, ≥ 99.9 %, Fisher Scientific; Ce(NO₃)₃·6 H₂O, ≥ 99.5 %, Fisher Scientific), before drying at 60 °C for 10 h and calcining at 700 °C for 5 h (1 °C min⁻¹ heating rate) to obtain the rare-earth oxide. Materials including ruthenium were impregnated for 14 h by a Ruthenium (III) nitrosyl nitrate solution (Ru(NO)(NO₃)_x(OH)_y, x+y=3, 1 % w/v, Fisher Scientific), then dried for 10 h at 60 °C before calcination at 350 °C for 5 h (1 °C min⁻¹ heating rate) to prevent the formation of toxic volatile ruthenium compounds. The process was repeated as necessary to reach the desired metal contents of 5 wt% Ru and 10 wt% REO (calculation example can be found in the SI). We selected 10 wt% REOs as the basic oxide promoter in our DFM study to provide a basis for direct comparison with other studies that have used 6–16 wt% alkali or alkali-earth oxides [4, 21–23]. This percentage is commonly used in the literature to optimize CO₂ adsorption and catalytic performance, and by using the same

loading for REOs, we aimed to evaluate their effectiveness relative to these more traditional promoters while maintaining consistency with established research practices. A relatively high ruthenium loading was chosen to distinguish the ruthenium-associated signals clearly during DRIFTS experiments. REOs concentration was chosen

Finally, the materials were labeled RuM/Al [M = REO (Gd₂O₃, Sm₂O₃, Nd₂O₃, CeO₂); Al = Al₂O₃] and stored in a desiccator. The final sample metal loading and the concentration of the stock nitrate solutions used to perform the impregnation were verified by ICP-OES.

2.2. Catalyst characterization

CO₂ temperature programmed desorption (CO₂-TPD) experiments were performed at atmospheric pressure using a catalyst characterization instrument with a thermal conductivity detector (TCD) (AMI-300, Altamira Instruments). Catalyst samples (100 mg) were pretreated in-situ under H₂ (99.999 % Linde) at 350 °C for 2 h. Then, CO₂ (15 vol%, 99.999 % Linde) was adsorbed at 40 °C for 60 min. Finally, the samples were purged under He flow (10 mL min⁻¹) for 60 min before heating to 800 °C (5 °C min⁻¹ ramp, hold for 30 min at max. temp.).

Specific surface area, total pore volume and pore size distribution of the catalysts were evaluated according to the BET method, Gurvitsch's rule (at $p/p_0 = 0.955$) and BJH (desorption branch) model, respectively, by N₂ adsorption-desorption measurements at -196 °C performed in a Micromeritics Gemini VII after degassing the samples overnight under He flow at 250 °C.

Isothermal H₂ chemisorption measurements were performed in a high vacuum sorption analyzer (Autosorb iQ, Anton Paar). 100 mg of catalyst were pretreated at 350 °C under a flow of pure H₂ (99.999 % Linde) for 2 h, then evacuated for 2 h at the same temperature and cooled under vacuum to 40 °C, where H₂ adsorption was performed in the pressure range 80–400 mmHg using the method of the double isotherm with an intermediary treatment under vacuum ($p = 0.001$ mmHg). Ru dispersion (D) was evaluated from the amount of strongly chemisorbed H₂, assuming a Ru:H stoichiometry equal to 1. The average particle size, d , was calculated from the dispersion assuming a Ru area of 6.135 Å²/Ru atom and a shape factor equal to 6. Results with confidence values based on repeated experiments on 30 % of the samples selected randomly can be found in Table 1.

X-ray diffraction (XRD) characterization of calcined and subsequently reduced samples was performed on a Bruker D8 Advance diffractometer equipped with a LYNXEYE linear position-sensitive detector (Bruker AXS, Madison, WI). Measurements were carried out using a continuous coupled 2θ/θ scan with Ni-filtered Cu Kα ($\lambda = 1.5418$ Å) radiation source with a tube voltage of 40 kV, current of 40 mA, and a 2 second sampling interval with 15° min⁻¹ rotation.

Transmission electron microscopy (TEM) was performed using a Thermo Scientific Talos F200X G2 (S)TEM to understand the catalyst microstructure and determine the Ru particle size. Fine powder of each sample was loaded onto a TEM grid (single-tilt holder 35°, ultrathin carbon film, Cu 200 mesh). The Ru mean particle size was determined by analysing the high-resolution images with the ImageJ software (version 1.53). For each sample, at least 200 particles were measured. In addition, Energy Dispersive X-Ray Spectroscopy (EDS) experiments were performed on the catalyst samples for elemental analysis. The accelerating voltage used was 200 kV.

X-Ray Photoelectron Spectroscopy (XPS) was conducted using a Thermo Scientific K-alpha instrument to obtain survey and high-resolution spectra of C1s, Al2p, O1s, Ru3d, Gd4d, Sm3d, Nd3d, and Ce3d elements. The powder samples were mounted on copper tape and degassed under vacuum for 15 hours before analysis. To minimize charging, a flood gun was employed, and the resulting survey and high-resolution spectra were charge-corrected relative to the C1s C–C peak at 284.5 eV.

Table 1

Sample overview: physicochemical properties of alumina support and Ru-REO based catalysts.

Sample	S_{BET}^a [m ² g ⁻¹]	V_{pore}^b [cm ³ g ⁻¹]	D_{pore}^c [nm]	H ₂ uptake [μmol g ⁻¹]	D [%]	d [nm]	CO ₂ uptake ^d [μmol g ⁻¹]	CO ₂ uptake ^e [mol mol _{REO} ⁻¹]
Al ₂ O ₃	270	0.92	5.0	-	-	-	84	-
Gd/Al	233	0.77	5.0	-	-	-	235	0.55
Sm/Al	215	0.70	5.2	-	-	-	273	0.66
Nd/Al	215	0.73	5.0	-	-	-	255	0.60
Ce/Al	227	0.71	5.0	-	-	-	183	0.17
Ru/Al	241	0.79	5.0	10.3	4.2	32	113	-
RuGd/Al	217	0.74	5.2	12.1	4.9	27	250	0.50
RuSm/Al	207	0.73	5.5	10.5	4.3	32	304	0.67
RuNd/Al	206	0.71	5.4	11.9	4.8	28	342	0.77
RuCe/Al	179	0.71	5.4	12.2	4.9	27	180	0.12

D = metal dispersion ± 0.4 %, d = metal crystallite size ± 4 nm, based on repeated analysis

^a S_{BET} = BET total specific surface area obtained from adsorption data in the 0.05–0.3 p/p^0 range; all reported data are within ± 10 m² g⁻¹ based on repeated analysis.

^b V_{pore} = pore volume was obtained at $p/p^0 = 0.97$.

^c D_{pore} = average pore diameter was calculated using Barrett-Joyner-Halenda (BJH) method.

^d = combined CO₂ uptake at 40 °C, measured by CO₂-TPD with a 3 % error based on repeated analysis.

^e = molar CO₂ uptake per mol of REO at 40 °C. Note: CO₂ uptake on Ru and Al₂O₃ is deducted.

2.3. Activity measurements

Operando thermogravimetric analysis (TGA) was performed during sequential CO₂ capture and direct methanation cycles using a Netzsch, TG 209 F1 Libra instrument. DFM samples ($m = 30 \pm 3$ mg) were pretreated under 20 vol% H₂ in Ar, at 350 °C for 1 h. Cycles were performed isothermally at 200 °C, the minimum temperature for methanation, by saturating the surface with 14 vol% CO₂ in Ar for 20 min before being exposed to 20 vol% H₂ in Ar for 30 min. This cycle was repeated 15 times with 5 min of Ar flush in between each step of CO₂ adsorption and hydrogenation (See Fig. 3). The gas outlet was monitored by a calibrated mass spectrometer (MS Hiden HPR 20, UK) for $m/z = 2$ (dihydrogen, H₂), $m/z = 15$ (methane, CH₄), $m/z = 18$ (water, H₂O), $m/z = 28$ (carbon monoxide, CO), $m/z = 44$ (carbon dioxide, CO₂) and argon as an internal standard with $m/z = 40$. The concentration of CO was calculated by subtracting the contribution of CO₂ from $m/z = 28$. 10 % of the experiments, selected at random, were repeated with a resulting error below 4 %.

2.4. DRIFTS measurements

Operando DRIFTS experiments were performed on a high-temperature DRIFT cell (Harrick fitted in Praying Mantis assembly). The spectrophotometer was a Nicolet 8700 (Thermo Fischer Scientific, Waltham, MA, USA) equipped with a liquid-N₂ cooled MCT detector. DRIFT spectra were recorded at a resolution of 4 cm⁻¹, and 8–32 scans were averaged. Products were analyzed using a transmission FTIR gas cell (17 mL) with a 10 cm path length kept at 60 °C to avoid product condensation. All experiments were conducted at ambient pressure and ramping temperature of 10 °C min⁻¹.

Two types of experiments were conducted for the *operando* catalytic test: (1) direct methanation between 350 and 200 °C and (2) CO₂ capture and hydrogenation cycles at a constant temperature of 200 °C. High-purity gases He (99.999 %), CO₂ (99.99 %), and H₂ (99.999 %) from Air Liquide were used for the tests, with all tests being carried out with a total flow rate of 43–50 mL min⁻¹.

On a typical methanation run, 10 mg of catalyst was loaded in the cell and reduced under 65 vol% H₂ in He at 350 °C for 1 h. Then, CO₂ was introduced at a ratio of 1:4:2 CO₂:H₂:He. After 5 min of spectra recording, the temperature was decreased stepwise every 25 °C (10 °C min⁻¹ ramp) until 200 °C, holding for 5 min at each temperature.

Sequential CO₂ capture and hydrogenation cycles were carried out on the same samples at 200 °C (isothermally) after surface pretreatment of 65 vol% H₂ in He, at 200 °C for 1 h. The chamber was then flushed with He for 5 min, and a DRIFTS background was recorded.

Subsequently, samples were saturated under 14 vol% CO₂ in He for 10 min. Next, the chamber was flushed with He for 5 min to remove any excess gaseous CO₂. Afterwards, samples were exposed to 65 vol% H₂ in He for another 10 min, and the chamber was then flushed with He for 5 min before introducing CO₂ again. The described cycle was repeated at least three times, while spectra were recorded every 0.5–2 min.

3. Results and discussion

3.1. Catalyst characterization

3.1.1. N₂ physisorption and H₂ chemisorption

The surface area of the alumina support was confirmed to be 270 m² g⁻¹ by N₂ adsorption/desorption measurements. Incorporating ruthenium into the alumina or REO/Al materials reduces the surface area by 10–30 % and pore volume by 10–20 %, potentially due to pore blockage by the relatively large Ru particles (Table 1). Ruthenium crystallite sizes were determined via hydrogen chemisorption to be around 30 nm for Ru/Al and Ru-REO/Al DFMs, with a metal dispersion of 4–5 %, which is independent of the presence of REOs (stoichiometry H/Ru = 1) [24].

3.1.2. TEM-EDS analysis

Transmission electron microscopy (TEM) coupled with energy dispersive spectroscopy (EDS) corroborated the metallic particle size and element distribution. Fig. 1 shows the TEM images (HAADF and elemental mapping) of the calcined Ru/Al and RuNd/Al (see supplementary information for the TEM images and particle size distribution histograms for the other samples in Figure S1 and Figure S2). In HAADF mode, REO (Nd₂O₃, Sm₂O₃, Gd₂O₃ and CeO₂) signals cannot be deconvoluted from the underlying signals of the Al₂O₃ support, thus preventing the determination of corresponding REO nanoparticle sizes. Yet, elemental mapping confirms that incorporating REOs via incipient wetness impregnation yields homogeneously dispersed rare-earth metals over the entire alumina support.

On the other hand, ruthenium appears to be dispersed in the form of larger crystallites, with some visible Ru-rich areas (small particles and clusters), in contrast to the well-dispersed REOs. However, no REO agglomeration was found around the ruthenium particles. The size distribution of the RuO₂ crystallites measured through TEM ranges from 20 to 60 nm with an average of 40 nm for Ru/Al and a slightly larger 50 nm average for RuNd/Al, which are of similar order to those calculated using hydrogen chemisorption (Table 1). Particle size distribution histograms measured by TEM for all tested DFMs can be found in the supplementary information (Figure S2), where the data highlight the variations in particle sizes across different DFMs. The rather large

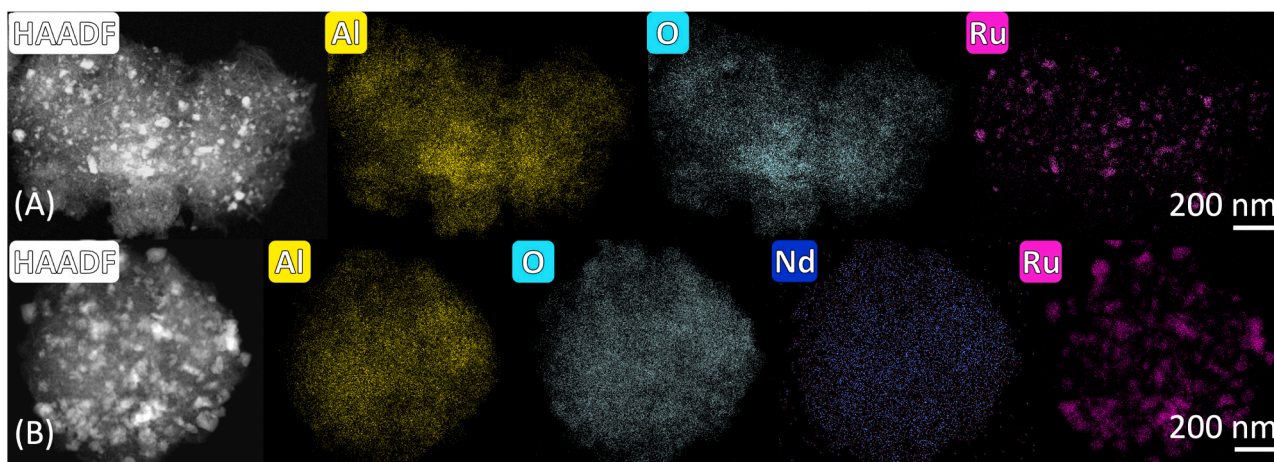


Fig. 1. TEM-EDS map imaging of the synthesized (A) Ru/Al and (B) RuNd/Al DFMs. The right insets show the size distribution of the Ru crystallite.

ruthenium crystallite sizes are a consequence of the relatively high Ru loading of 5 wt%, which aligns with previous observations of a correspondent increase of metal particle sizes when Ru is loaded above 0.1 wt % on alumina [25]. Methanation is a structure-dependent reaction, and ruthenium particles of 1–4 nm are preferred to ensure high catalytic activity and CH_4 selectivity [26]. Nevertheless, crystallite sizes around 30–40 nm are not uncommon and it has been shown that at these crystallite sizes, ruthenium-alumina catalysts are mostly selective towards CH_4 formation [25,27]. Moreover, Ru metal content was selected to maximize IR signals for the in-situ DRIFTS analysis and to compare to similar previously reported alkali-based DFMs (e.g. 5 wt%Ru-6.1 wt% Na_2O /Al $_2\text{O}_3$) in literature [5].

3.1.3. XRD analysis

X-ray diffraction patterns were obtained of the used support and REO/Al materials after calcination, and those of Ru/Al and all synthesized Ru-REO/Al DFMs after calcination and hydrogen pretreatment (Fig. 2). The alumina support exhibits a diffraction profile that confirms the presence of only γ -Al $_2\text{O}_3$, with a combination of broad low-intensity and sharp high-intensity peaks, characteristic of a partially crystalline solid (Al $_2\text{O}_3$ relative crystallinity = 58 %, Table S1). Examples of XRD peak deconvolutions can be found in the supplementary information, specifically in Figure S3 for Gd/Al and Figure S4 for Ru/Al. After REO addition, the distinctive peaks of Gd $_2\text{O}_3$, Sm $_2\text{O}_3$, and Nd $_2\text{O}_3$ expected in the ranges of 25–35° and 40–60° 2 θ , were not visible for either REO/Al or Ru-REO/Al materials. This suggests that these REOs are either in the amorphous phase or are present as nano-dispersed (< 5 nm) crystallites, as observed by TEM-EDS imaging and confirmed when calculating the relative crystallinity of the materials (30 % decrease compared to Al $_2\text{O}_3$). In the case of materials containing CeO $_2$, distinguishable sharp peaks are found at 28.5°, 33.1°, 47.5°, and 56.3° 2 θ , indicating the existence of a crystalline phase. The presence of the CeO $_2$ crystalline phase boosted the relative crystallinity of Ce/Al and RuCe/Al to 70 % and 81 %, respectively. Although, through nanoscale TEM imaging, CeO $_2$ particles appear to be as well-dispersed as other REOs (Figure S1), their increased crystallinity should be considered when looking at the data presented in the upcoming sections. While all tested materials adsorb CO $_2$ by a similar mechanism, RuCe/Al repeatedly presents lower CO $_2$ adsorption and, consequently, lower methane formation than the rest of the tested REOs materials.

When ruthenium is introduced to the support, an intense peak appears at 44°, with three low-intensity peaks emerging at 58.3°, 69.5°, and 78.5° 2 θ (not visible due to scale). These peaks are attributed to elemental ruthenium, with no additional peaks that could hint at the presence of RuO $_2$, corroborating the efficacy of the selected hydrogen pretreatment. In the cases where Ru and REOs are both present, the four

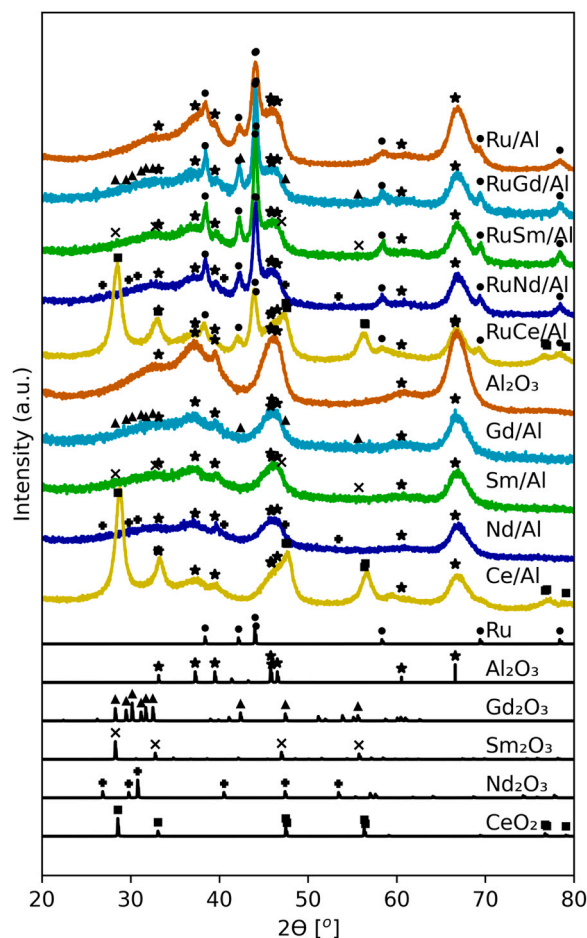


Fig. 2. XRD patterns of REO catalyst for (A) without and (B) with Ru. Reference patterns of γ -Alumina (PDF# 047-1308), Ru (PDF# 006-0663), Gd $_2\text{O}_3$ (PDF# 012-0474), Sm $_2\text{O}_3$ (PDF# 015-0813), Nd $_2\text{O}_3$ (PDF# 006-0408), and CeO $_2$ (PDF# 004-0593), respectively.

peaks corresponding to metallic Ru are still distinguished [15]. In all cases, no peaks belonging to nitrogenous species, or any other undesired phases were observed, confirming that the surface was properly cleaned during calcination. For reference, we compared the obtained XRD spectra against possible REO-Al alloys and found no matching peaks, confirming that the existence of alloys is not likely (Figure S5). Since the

presence of REOs could not be fully confirmed by XRD, we conducted XPS analysis. Based on XPS results, rare-earth metals on the catalyst surface are present in their expected oxidation states: Gd as Gd^{3+} , Sm as Sm^{3+} , Nd as Nd^{3+} , and Ce as Ce^{4+} and Ce^{3+} (characteristic of CeO_2). This is illustrated in Figure S6, where the Gd4d, Sm3d, Nd3d, and Ce3d spectra confirm these oxidation states. Additionally, Figure S7 provides further insights into the effects of REO addition on the Al2p and O1s binding energies, highlighting the formation of AlO_x suboxides and oxygen vacancies. The Ru3d spectra in the same figure also demonstrate variations in ruthenium's electronic environment depending on the specific REO added.

3.1.4. CO_2 -TPD

To assess the surface basicity of the prepared DFMs, CO_2 -TPD was carried out with an adsorption temperature of 40 °C. Fig. 3 reveals that most CO_2 molecules are adsorbed on weak and moderate basic sites [21, 28], inferred from desorption below 250 °C and between 300 – 650 °C, respectively. No desorption above 650 °C was identified, demonstrating an absence of strong and highly stable basic sites across all samples.

Fig. 3A presents the CO_2 -TPD profiles for REO/ Al_2O_3 samples without Ru. Blank Al_2O_3 consists predominately of weak basic sites, indicated by CO_2 desorption peak at around 100 °C. The adsorption on these weak sites is enhanced by REO addition, which translates into bigger peaks in the 50 – 250 °C temperature range (i.e., shoulder at 200 °C) [29], which is also visualized/quantified in Fig. 4. Moderate interactions appear with the addition of REOs, with Sm and Nd showing peaks at around 400 °C, and Gd at 420 °C and 550 °C, while Ce showing an almost negligible peak at 350 °C. The CO_2 -desorption profile for the Gd_2O_3/Al_2O_3 (short Gd/Al) sample displays a peak at higher temperatures, which correlates to stronger basic sites compared to Sm/Al, Nd/Al and Ce/Al.

Ru-REO/ Al_2O_3 CO_2 -desorption patterns are illustrated in Fig. 3B. Surprisingly, the number of moderate basic sites seems to increase significantly, indicated by the larger CO_2 desorption peak for RuGd/Al, RuSm/Al and RuNd/Al at around 400 °C. Similar desorption temperatures have been reported for Ru/ Gd_2O_3 and Ru/ Sm_2O_3 catalysts [10]. These moderate strength sites have been previously attributed to the formation of defect sites with stronger basicity [30]. In the present case, the enhanced CO_2 uptake between 300 – 500 °C for the Ru-containing samples is most likely attributed to the creation of surface defects (e.

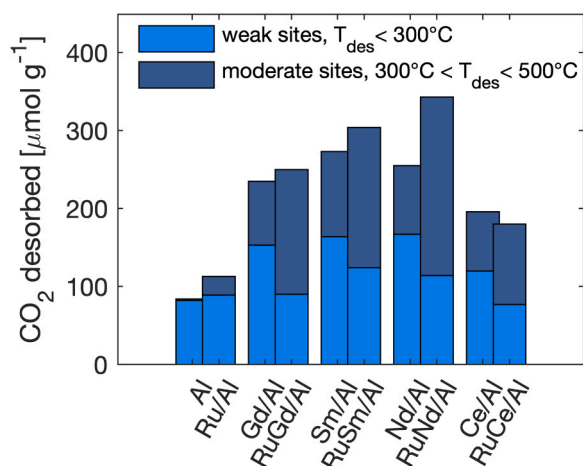


Fig. 4. CO_2 desorption results for Ru-REO/Al and REO/Al materials.

g., oxygen vacancies) on the REOs during the impregnation with the acidic Ru precursor (ruthenium nitrate solution), and to minor part during the hydrogen pretreatment. To confirm this, a Sm/Al samples was prepared and treated with nitric acid (HNO_3) during the impregnation to simulate the acidity of the ruthenium nitrate precursor solution. The corresponding CO_2 -TPD in Figure S8 shows a much larger CO_2 desorption peak in the range of 400 °C to 500 °C for the nitric acid treated sample than for the standard prepared Sm/Al sample (i.e., Sm/Al (10 wt% HNO_3 vs. Sm/Al(H_2O)).

Fig. 4 presents the amount of desorbed CO_2 on both weak and moderate basic sites, where RuNd/Al shows the largest total uptake over the entire temperature profile. The presented data confirms that CO_2 adsorption occurs mainly on weak basic sites for the alumina support, and the inclusion of ruthenium modestly increases adsorption on both weak and moderate sites. The total CO_2 uptake on bare alumina and the Ru/Al catalyst is $84 \mu mol g^{-1}$ and $113 \mu mol g^{-1}$, respectively. This 30 % improvement in CO_2 uptake for catalysts containing 5 wt% ruthenium vs. the pure support is in agreement with what has been reported by other authors [28].

Similar observations can be made for the rest of the tested materials. For all REO/ Al_2O_3 samples, REO addition introduces moderate basic

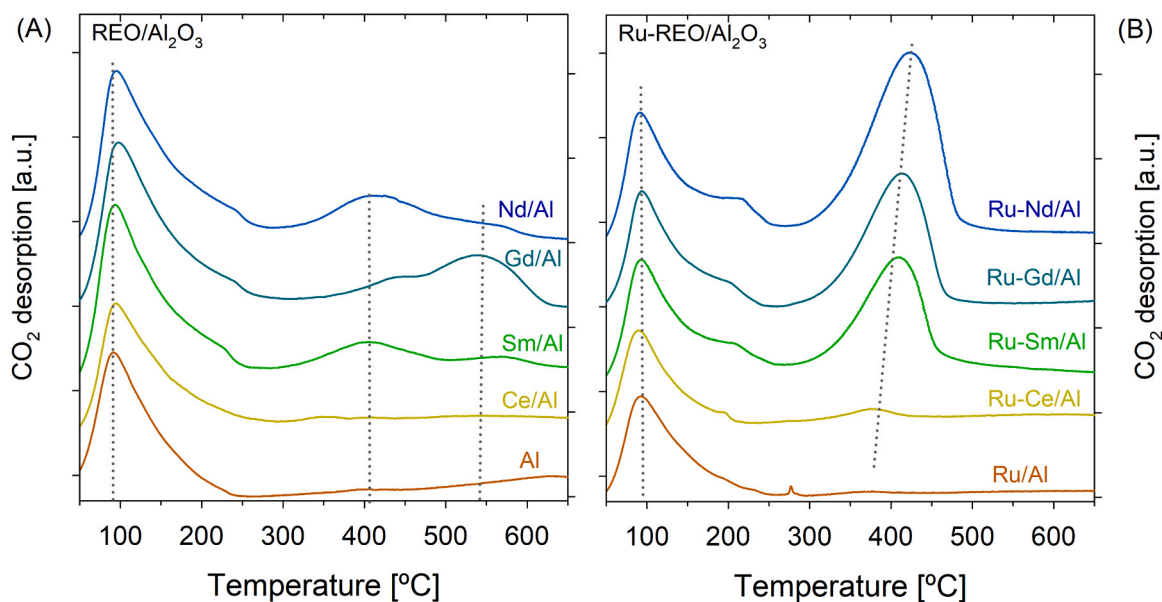


Fig. 3. CO_2 -TPD profiles of (A) REO/ Al_2O_3 and (B) Ru-REO/ Al_2O_3 materials. Conditions: ~ 100 mg of catalyst, CO_2 saturation at 40 °C, and temperature ramp 5 °C min^{-1} .

sites, but more than half of the adsorption occurs on weak basic sites. Compared to the alumina support, double the amount of CO₂ is adsorbed on weak sites for Gd/Al, Sm/Al, and Nd/Al samples, except for Ce/Al, which has a CO₂ uptake increase of only 46 %. As per the moderate basic sites, CO₂ adsorption increased drastically for REO/Al₂O₃ samples, going from just 2 μmol g⁻¹ on Al₂O₃ to a maximum of 109 μmol g⁻¹ on Sm/Al. On the other hand, adding ruthenium to REO/Al materials decreased the adsorption on weak basic sites, while increasing it on moderate sites due to the formation of oxygen vacancies, which enhances CO₂ adsorption.

Overall, the CO₂-uptake for Ru-REO/Al₂O₃ catalysts decreased in the following order: RuNd/Al > RuSm/Al > RuGd/Al > RuCe/Al > Ru/Al. In the case of RuNd/Al, the REO-ruthenium-alumina interactions seem to be exceptionally favorable for CO₂ adsorption, reaching a total uptake of 342 μmol g⁻¹, which is three times larger than that of Ru/Al. On the contrary, the addition of cerium oxide does not significantly increase the CO₂ uptake, reaching a value only 50 % larger of 180 μmol g⁻¹. These results are of similar magnitude to what has been reported for alkali-containing DFMs (480 μmol g⁻¹ of CO₂ adsorption over 5 wt%Ru-6.1 wt%“Na₂O”/Al₂O₃ [1]), proving that REOs are a competitive candidate for DFM applications.

On a molar basis, the CO₂ uptake is very high with 0.77 mol_{CO2} mol_{Nd2O3}⁻¹, 0.67 mol_{CO2} mol_{Sm2O3}⁻¹ and 0.5 mol_{CO2} mol_{Gd2O3}⁻¹ (Table 1), which indicates and confirms the very small and well-dispersed nature of the REO within the alumina support apart from the CeO₂ sample. In contrast, the 5 wt%Ru-6.1 wt%“Na₂O”/Al₂O₃ sample from study [28] has a much smaller molar-based CO₂ uptake of around 0.3 mol_{CO2} mol_{Na2O}⁻¹.

3.2. TGA CO₂ uptake – hydrogenation cycles

The Ru-REO/Al₂O₃ material's performance as DFMs was tested by isothermal CO₂ capture and subsequent methanation cycles in a TGA instrument. Fig. 5 shows the mass change during a complete cycle for the reduced Ru/Al (top) and RuNd/Al (bottom), operating at 200 °C to maximize CO₂ adsorption, while being able to produce methane. Fifteen

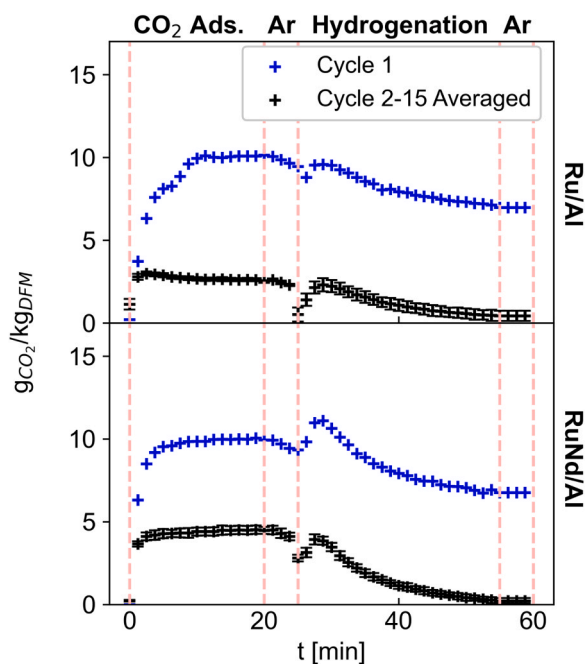


Fig. 5. Relative mass change profiles during the first CO₂ adsorption and hydrogenation cycle (blue) and the average of cycles 2–15 (black) for the reduced Ru/Al and RuNd/Al samples at 200 °C. The red-dashed lines denote different cycle sections.

sequential cycles were performed, each cycle lasting 60 minutes. After 1 h pretreatment under 20 vol% H₂/Ar, an adsorption period was performed by introducing 14 vol% CO₂/Ar for 20 min (first section), followed by a 5 min Ar flush (second section). Then, the hydrogenation period begins by starting a 20 vol% H₂/Ar stream that continues for 30 min (third section), followed by another 5 min Ar flush where no mass change is recorded (fourth section).

During the CO₂ adsorption period, gas molecules bind to the surface on the oxide basic sites as carbonates (*vide infra* DRIFTS data in Fig. 8) [31]. Any weakly bound CO₂ desorbs from the surface during the first argon purge. Nevertheless, thanks to the existence of weak and moderate interactions at 200 °C, a significant fraction of CO₂ remains on the surface and reacts when H₂ is introduced to CH₄.

In all cases, right after the pretreatment step, a large mass increase is observed (blue markers). This higher uptake during the first cycle is attributed to the existence of oxygen vacancies on the REO surface, creating new adsorption sites available, as discussed in the previous section. During the following cycles (black markers, working capacity), the CO₂ uptake capacity diminishes as these extra moderate adsorption sites get saturated, and no oxygen vacancies are created during the hydrogenation step. Therefore, the difference between the maximum uptake and working capacity of the tested DFMs is attributed to captured CO₂ molecules that are not able to leave the surface at 200 °C.

In agreement with CO₂-TPD results, RuNd/Al showed greater thermal stability, being able to adsorb and retain more CO₂ than Ru/Al throughout the saturation time. This can be confirmed when comparing the CO₂ adsorption sections in Fig. 5. For Ru/Al, during cycles 2–15, the CO₂ uptake curve reaches an initial maximum of 2.7 g_{CO2} kg_{DFM}⁻¹ after 3 min of CO₂ uptake, which then slightly decreases over time and stabilizes at 2.3 g_{CO2} kg_{DFM}⁻¹ after 10 min under adsorption conditions. In contrast, the homologous curve for RuNd/Al reaches an initial value of 3.9 g_{CO2} kg_{DFM}⁻¹ after 3 min under the CO₂ feed, and it continues to increase until it plateaus and remains constant at 4.3 g_{CO2} kg_{DFM}⁻¹ after 15 min of adsorption.

Looking at the hydrogenation section, weight decreases until reaching a plateau. The steep slope for RuNd/Al, indicates that CO₂ reacts with hydrogen as soon as it reaches the surface, discarding any mass transfer limitations. In contrast, methane production over Ru/Al has a higher variance over cycles 2–15, which is displayed by bigger error bars. In both cases, no CO₂ and a negligible amount of CO is detected during H₂ addition, corroborating that most desorbed CO₂ is converted to CH₄ and validating previously reported assumptions of Ru being a great CO₂ hydrogenation catalyst at low temperatures [5]. The slight decrease, followed by an increase in weight during the hydrogenation section, is an experimental artifact generated by the initiation of the hydrogen mass flow controller in the TGA. The cycled experiment is reproduced under the same conditions with an empty crucible, and a similar behaviour is observed, linking part of this response to a buoyancy effect intrinsic to the instrument (Figure S9). Similar cycled experiments are conducted for the support alone (Figure S9) and all tested catalysts (Figure S10), with RuNd/Al being the best-performing material.

Fig. 6 (A-E) shows the CO₂ adsorption capacity (yellow circles), methane production (green bars), and CO₂ desorption during the post-CO₂-capture argon flush (gray bars) for every Ru-REO/Al DFM. For cycles 2–15, mass gain/loss from CO₂ adsorption and methane production remained relatively constant. For example, for Ru/Al, CO₂ uptake was 49 and 47 μmol g⁻¹ on average during the initial cycles (3–8) and the final cycles (9–15), respectively. Thus, a 2 % decrease in CO₂ capture throughout the length of the experiment was observed (~14 h in stream). For Ru-REO/Al DFMs, this number remained within 4–7 %.

During the subsequent argon flush, weakly bound CO₂ desorbed from the DFM surface, resulting in the loss of ~20 % of the total uptake. Hydrogen introduction produces CH₄ with a low amount of CO (<4 % of total product stream for Ru-REO/Al DFMs, Table 2) and regenerates the DFM in the 30 min exposure span. In the end, after each cycle, samples

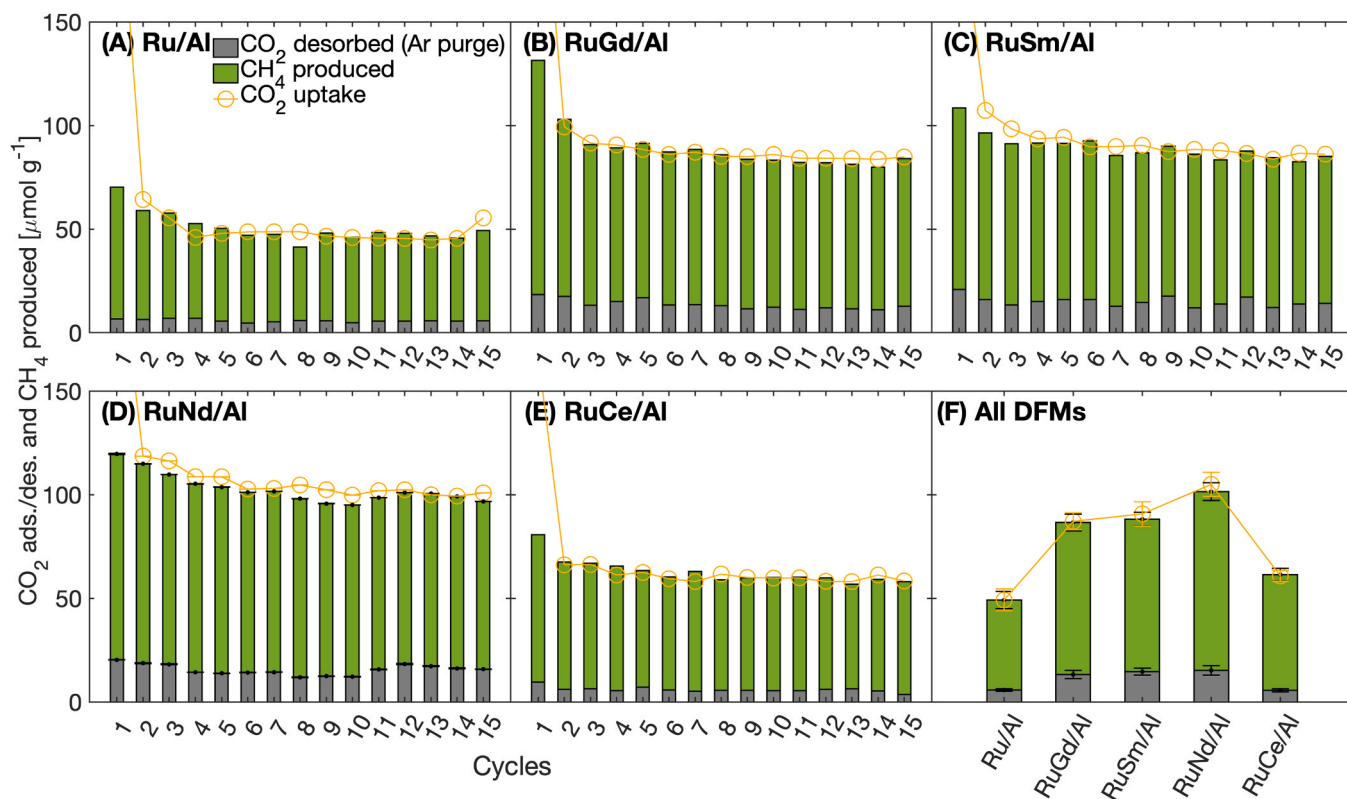


Fig. 6. Results for isothermal CO_2 adsorption/desorption and CH_4 production: (A-E) 15 cycles per DFM; (F) averaged over cycles 2–15 for different DFMs. Note: The amount of CO desorbed during the hydrogenation is not visualized; see selectivity values in Table 2.

Table 2

Summary of TGA cycled tests on Ru-REO/Al.

Sample	CO_2 adsorbed [$\mu\text{mol g}^{-1}$]	CH_4 produced [$\mu\text{mol g}^{-1}$]	CO_2 desorbed (Ar purge) [$\mu\text{mol g}^{-1}$]	Carbon balance [%]	X_{CO_2} [%]	S_{CH_4} [%]	Y_{CH_4} [%]
Ru/Al	49.2	37.3	6.6	102	88	86	88
RuGd/Al	87.2	71.2	13.2	99	84	97	96
RuSm/Al	90.7	73.3	14.6	97	81	97	96
Al							
RuNd/Al	109.0	85.0	15.4	93	80	98	91
RuCe/Al	60.8	52.9	5.7	101	92	95	96

All reported data was obtained by averaging cycles 2 – 15. Error based on repeated analysis is within $\pm 2\%$.

can re-adsorb CO_2 on the sites that deplete during methane production [32].

Fig. 6F summarizes the average performance over 15 cycles for all Ru-REO/Al samples at 200 °C. In accordance with CO_2 -TPD results, the CO_2 adsorbed during the cycles on Ru-REO/Al catalysts decreased in the same order, confirming that the addition of REOs enhances Ru-DFM performance. Carbon balance discrepancies can be attributed to CO_2 retained in the sample that could react under higher H_2 partial pressures. DRIFT studies on Ru-REO/Al samples under similar CO_2 capture and hydrogenation conditions show inactive carbonate species that can form on the catalyst surface when Ru catalyzes a methanation reaction over CO_2 -saturated materials. Another explanation for the partial carbon balance might be the presence of moderate to strong CO_2 interactions with the Ru-REO DFMs surface, as shown in the CO_2 TPD results (Figure 3Figure). The existence of moderate basic sites, as well as carbonate species on the Ru-REO DFMs surface, can result in unreacted CO_2 that cannot be hydrogenated at 200 °C, as it will be confirmed in the DRIFTS section. At the working temperature of 200 °C, all tested catalysts were able to adsorb and react reversibly 30 – 45 % of the total CO_2 uptake measured by CO_2 -TPD (Table 1), indicating that the initial oxygen vacancies are filled (i.e., during the first CO_2 adsorption and

carbonate formation) and are not recreated during the cycle experiments.

Based on CO_2 adsorption and methane production capacities, the DFM containing 10 wt% Nd_2O_3 and 5 wt% Ru had the highest CO_2 uptake (109 $\mu\text{mol g}^{-1}$) and generated the most methane (85 $\mu\text{mol g}^{-1}$) compared to other REO adsorbents with the same loading. The best and worst performing Ru-REO/Al O_3 samples were RuNd/Al and RuCe/Al with 120 % and 24 % more CO_2 adsorption capacity than Ru/Al. All Ru-REO/Al materials had a methane production of 56–85 $\mu\text{mol g}^{-1}$, surpassing recently reported values obtained for alkali and alkali-earth promoted Ru-based materials operated at 250 °C [33]. This highlights the advantages of using REOs, as we can achieve significant activity at the lower temperature of 200 °C.

3.3. DRIFT spectroscopy

3.3.1. CO_2 hydrogenation at 200 °C

Operation DRIFT experiments were carried out to better understand the surface reactions happening over the Ru-REO/Al samples. Samples were first tested under direct CO_2 hydrogenation conditions ($\text{CO}_2:\text{H}_2 = 1:4$) at various temperatures ranging between 350 – 200 °C (data not

shown) before DFM sequential tests. Fig. 7 visualizes the infrared spectra upon heating the samples (Ru/Al, RuGd/Al and RuCe/Al) in H₂ atmosphere at 200 °C after being exposed to a CO₂ and H₂ feed. Linear and bridged CO adsorbed on Ru are observed at 2040 cm⁻¹ and 1960 cm⁻¹ (Table 3), respectively. The bridge bond refers to linearly CO adsorbed on Ru co-adsorbed with an adjacent O-Ru bond [10,34]. At wavenumbers 2904 cm⁻¹, 1590 cm⁻¹ and 1394 cm⁻¹, formate bands are observed corresponding to $\nu(\text{C-H})$, asymmetric $\nu_{\text{as}}(\text{OCO})$ and symmetric $\nu_{\text{s}}(\text{OCO})$ vibrations, respectively [35]. These species are known to form over ruthenium-alumina catalysts during methanation reactions and are stable under H₂ atmosphere. The spectrum of these highly stable species was thus part of the DRIFTS background collected afterwards before the cycled CO₂ adsorption and hydrogenation experiments.

3.3.2. CO₂ adsorption at 200 °C

Upon the CO₂ addition over the DFM samples, several IR bands are visible, as visualized in Fig. 9 and summarized in Table 3, for peak identification within the wavenumber range of 2200 cm⁻¹ to 1100 cm⁻¹. An extended range up to 4000 cm⁻¹ is illustrated in Fig. 11, which shows multiple peaks at 3730, 3700, 3630, 3600 and 2300 cm⁻¹. The IR band at ~3700, 3600 and 2300 cm⁻¹ refer to CO₂ overtones, while the peaks 3730 and 3630 cm⁻¹ are associated with O-H stretching of bicarbonates [34,36]. As expected during the CO₂ saturation, no IR band at 3020 cm⁻¹ for the C-H stretch vibration of CH₄ is observed.

CO₂ dissociatively adsorbs on Ru mostly in the form of linear bonded CO as indicated by the characteristic vibrations at 2020 cm⁻¹, whereas the bridge bonded CO is only visible as a shoulder at 1960 cm⁻¹. The four peaks at around 1650 cm⁻¹, 1540 cm⁻¹, 1440 cm⁻¹ and 1330 cm⁻¹ refer to various carbonate and bicarbonate species. For example, the band at 1650 cm⁻¹ and 1440 cm⁻¹ are the asymmetric and symmetric O-C-O stretching [$\nu_{\text{as}}(\text{CO}_3)$ and $\nu_{\text{s}}(\text{CO}_3)$] of potential adsorbed bicarbonate (HCO₃), which are formed during the reaction of CO₂ and surface hydroxyl species [4,34,37]. The hydroxyl $\delta(\text{OH})$ -band is usually visible at ~1225 cm⁻¹; however, due to the high temperature of 200 °C, the peak is not visible, which has also been observed over Ru/Sm₂O₃ and Ru/Gd₂O₃ catalyst [10] and over Y₂O₃ catalyst [36]. The IR bands at around 1540 cm⁻¹ and 1430 cm⁻¹ refer likely to the asymmetric and symmetric O-C-O stretching [$\nu_{\text{as}}(\text{CO}_3)$ and $\nu_{\text{s}}(\text{CO}_3)$] of bidentate carbonate (b-CO₃). No IR band associated with monodentate carbonates (m-CO₃) is visible, which have been observed at lower temperatures (i. e., 50 °C) during CO₂ adsorption over Sm₂O₃, Gd₂O₃ and Y₂O₃ at around 1065 cm⁻¹ [10].

For the 5 wt% Ru/Al sample, the predominate CO₂ adsorption peak is over the Ru active site (Ru-CO, at 2040 cm⁻¹), while peaks associated with the formation of bicarbonates and carbonates are smaller. As expected, over the 10 wt% Gd/Al sample, no Ru-CO peak is visible, whereas the bicarbonates and carbonates bands are much larger, confirming the existence of additional CO₂ adsorption sites on the rare earth

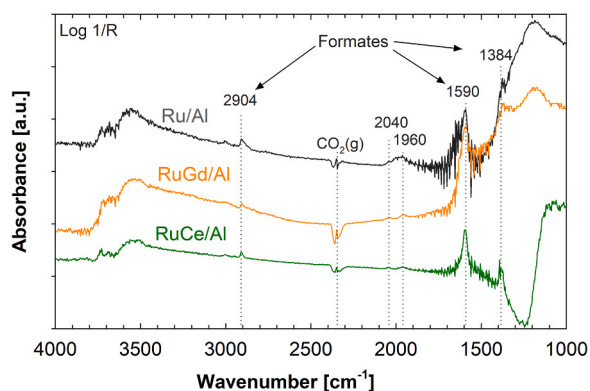


Fig. 7. DRIFTS Spectra of Ru-REO/Al DFMs under H₂ after the reaction under a CO₂ + H₂ feed at 200 °C. KBr was used as background.

metal oxide. For the RuGd/Al and RuSm/Al samples, the bicarbonates and carbonates IR bands have about the same intensity as the Ru-CO band. In contrast, the bicarbonates and carbonates intensities for the RuNd/Al sample are higher. For the RuCe/Al sample, the bicarbonates and carbonates intensities are smaller than those of the Ru-CO band (Fig. 8). These results are in agreement with the CO₂-TPD data, showing the order of CO₂ adsorption as RuNd/Al > RuSm/Al > RuGd/Al > RuCe/Al > Ru/Al.

3.3.3. Sequential CO₂ adsorption and hydrogenation at 200 °C

DRIFTS spectra were obtained at 200°C over reduced Ru/Al, Ru-REO/Al DFMs, and Gd/Al during the exposure to CO₂ (10 min), followed by He purge (5 min), and then H₂ (10 min) (Fig. 9). On the materials where ruthenium metal is present, the surface gets readily covered with Ru carbonyl species (band around 2015 cm⁻¹ for Ru/Al and 2022 cm⁻¹ for Ru-REO/Al). In contrast, the spectra obtained over Gd/Al do not show the presence of carbonyl species (Fig. 9F). Additionally, for all samples, various carbonates could be observed, and their plausible classification can be found in Table 3. The fact that Ru-CO was observed on the Ru-containing samples indicates that CO₂ was readily decomposed over the elemental metal that was still probably covered with hydrogen at the time CO₂ was introduced. Upon CO₂ exposure, both Ru-CO and carbonate signals rapidly grew and remained constant under the CO₂-containing atmosphere, albeit Ru-CO was quicker to get to the steady-state value (Fig. 10).



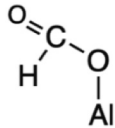
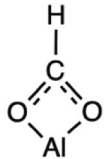
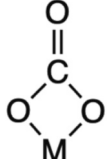
To further understand the behavior of each material under the varying gas feed, the heights of all peaks present in Fig. 9 were normalized to their maximum and are shown as a function of time in Fig. 10. For Ru/Al, the signal of carbonates (b-CO₃) and bicarbonates (HCO₃) decreased drastically once CO₂ was removed from the feed and was essentially null after the 5 min purge. This shows that the basicity of alumina is too weak to retain carbonates at 200 °C. As opposed to this, in the cases where an REO is present on the surface, most of the adsorbed carbonates prevail during the He flush. These observations warrant the use of REOs that are known to be basic to favour the retention of carbonates on the DFM even after CO₂ is no longer being fed. On the other hand, the Ru-CO band remains essentially constant for both Ru/Al and Ru-REO/Al samples, showing that carbonyls are strongly bound to Ru atoms regardless of the presence of REOs. In all cases, ruthenium carbonyls are rapidly removed from the surface upon H₂ introduction, leading to methane formation. This data indicates that methane formed over Ru/Al was mostly due to CO adsorbed on Ru and not alumina-bound carbonates. Over Ru-REO/Al samples, CH₄ can be produced through the reaction of ruthenium carbonyls, as well as carbonates that potentially spill over to a nearby ruthenium site.

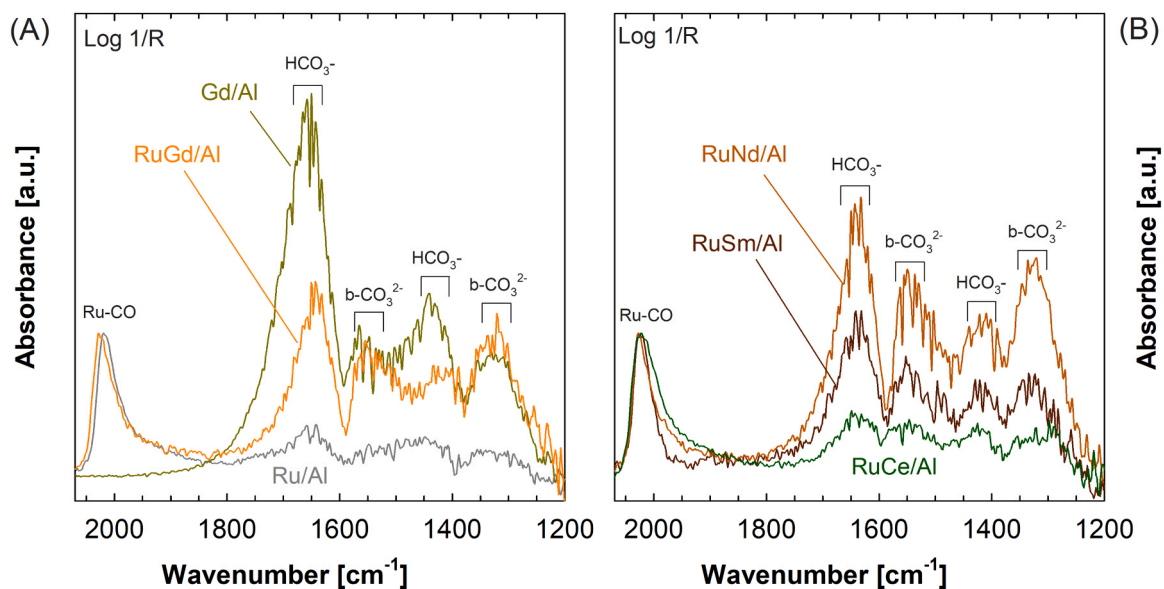
All Ru-REO/Al showed large bands in the 1800–1200 cm⁻¹ region due to various carbonate species. It is worth to note that the Sm, Gd and Nd-promoted samples in the presence of CO₂ showed carbonate bands with an intensity higher than that of the Ru-CO, in contrast to the case of the Ru-Ce and non-promoted Ru samples. The carbonate bands of these three samples were still of an intensity similar to that of the Ru-CO band after carbon dioxide was removed, indicating significant retention of adsorbed CO₂. These observations are consistent with the kinetic results reported in the previous section.

The treatment under H₂ of RuNd/Al was looked into detail since this sample exhibited the highest carbonate signal just before H₂ introduction (Fig. 11).

Interestingly, no evidence of formate species, with a C-H stretching band around 2900 cm⁻¹, could be observed. The decay of Ru-CO at 2022 cm⁻¹ and that of the carbonates occurred on a similar timescale, with the bridged species occurring somewhat faster than that of the monodentate species. These observations indicate that the transport of carbonate species from the REO to the Ru particles is faster than the hydrogenation of the carbonyl species to yield methane. (N.B. if it were the contrary, no Ru-CO could be observed). Therefore, the rate-determining step is carbonyl hydrogenation, e.g., the first H addition

Table 3Peak assignment (wavenumber in cm^{-1}) of spectra from *operando* DRIFRS study (refer to Figs. 7, 8 and 9).

Surface species	Structure	$\nu(\text{Ru-CO})$ [cm^{-1}]	$\nu_{\text{as}}(\text{CO}_3^-)$ [cm^{-1}]	$\nu_s(\text{CO}_3^-)$ [cm^{-1}]	$\nu(\text{OH}); \delta(\text{OH})$ [cm^{-1}]	$\nu(\text{C-H})$ [cm^{-1}]
Linear CO adsorption, Ru-CO		2044–2015	-	-	-	-
Linear oxygen adsorption, Ru-O		1960	-	-	-	-
Formates, HCOO^-		-	1594	1393	-	2905
Bicarbonate, HCO_3^-		-	1650–1640	1440–1410	3740; 3640; 1220 [#]	-
Bidentate carbonate, b-CO_3^{2-}		-	1545–1544	1330–1320	-	-

[#] d(OH) 1220 cm^{-1} , not visible**Fig. 8.** In-situ DRIFTS during CO_2 adsorption at $200 \text{ }^\circ\text{C}$, over (A) Ru/Al, Gd/Al, RuGd/Al and (B) RuSm/Al, RuNd/Al and RuCe/Al samples.

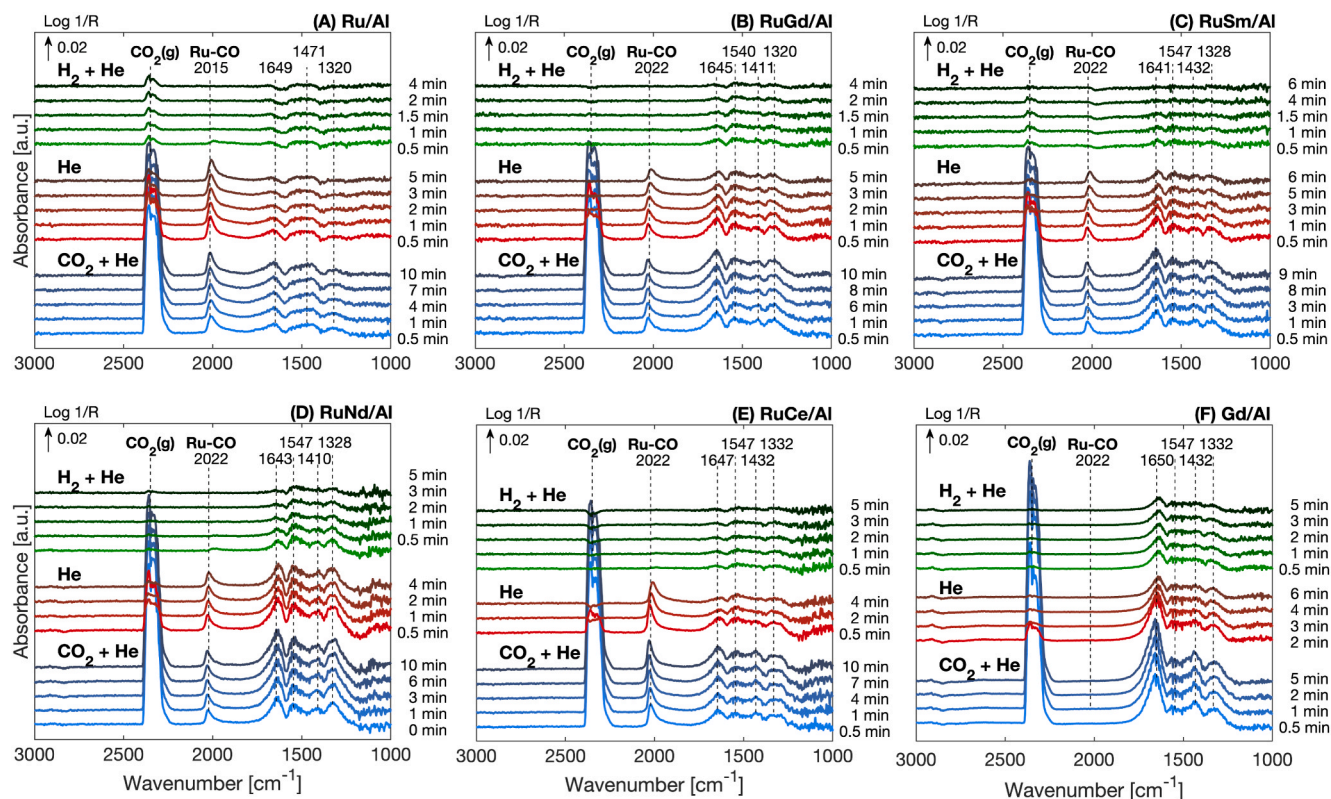


Fig. 9. DRIFTS Spectra of Ru/Al, Ru-REO/Al DFMs and Gd/Al during full sequence of exposure to CO₂ for 10 min (blue), followed by 5 min purge in He (red) and 10 min under H₂ (green) at 200 °C. The DRIFTS background was collected on each sample when reduced at 200°C just before CO₂ adsorption.

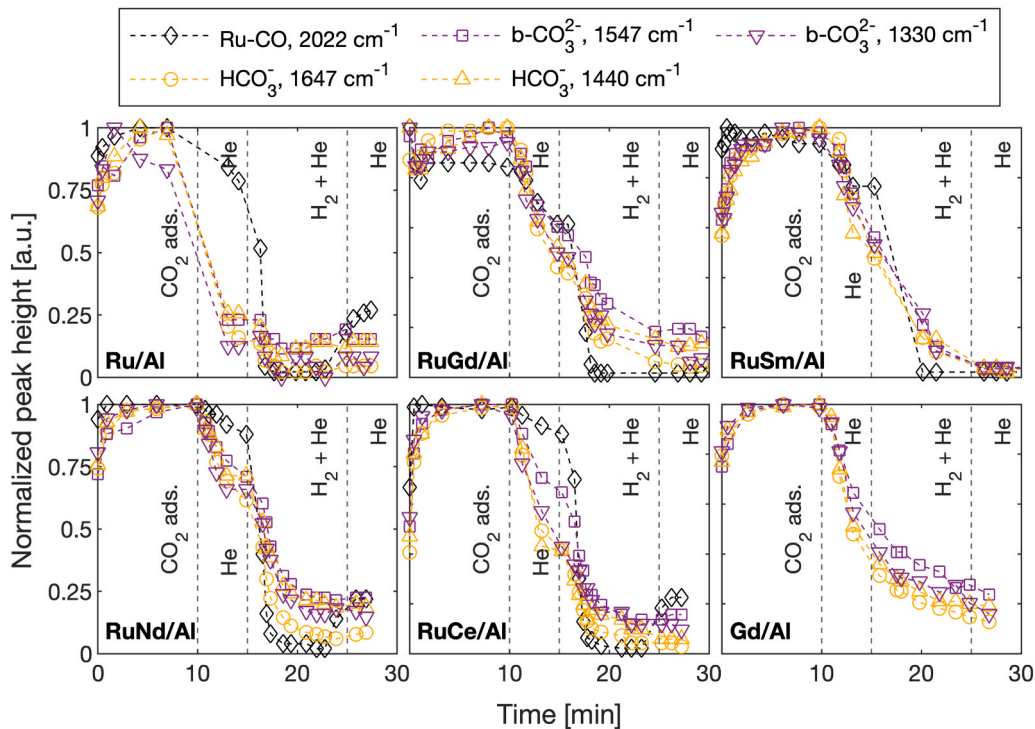


Fig. 10. Normalized peak heights as a function of time. Conditions: CO₂ ads. = 14 vol% CO₂ in He; H₂ + He = 65 vol% H₂ in He; total flow rate = 43–50 mL min⁻¹ at 200 °C.

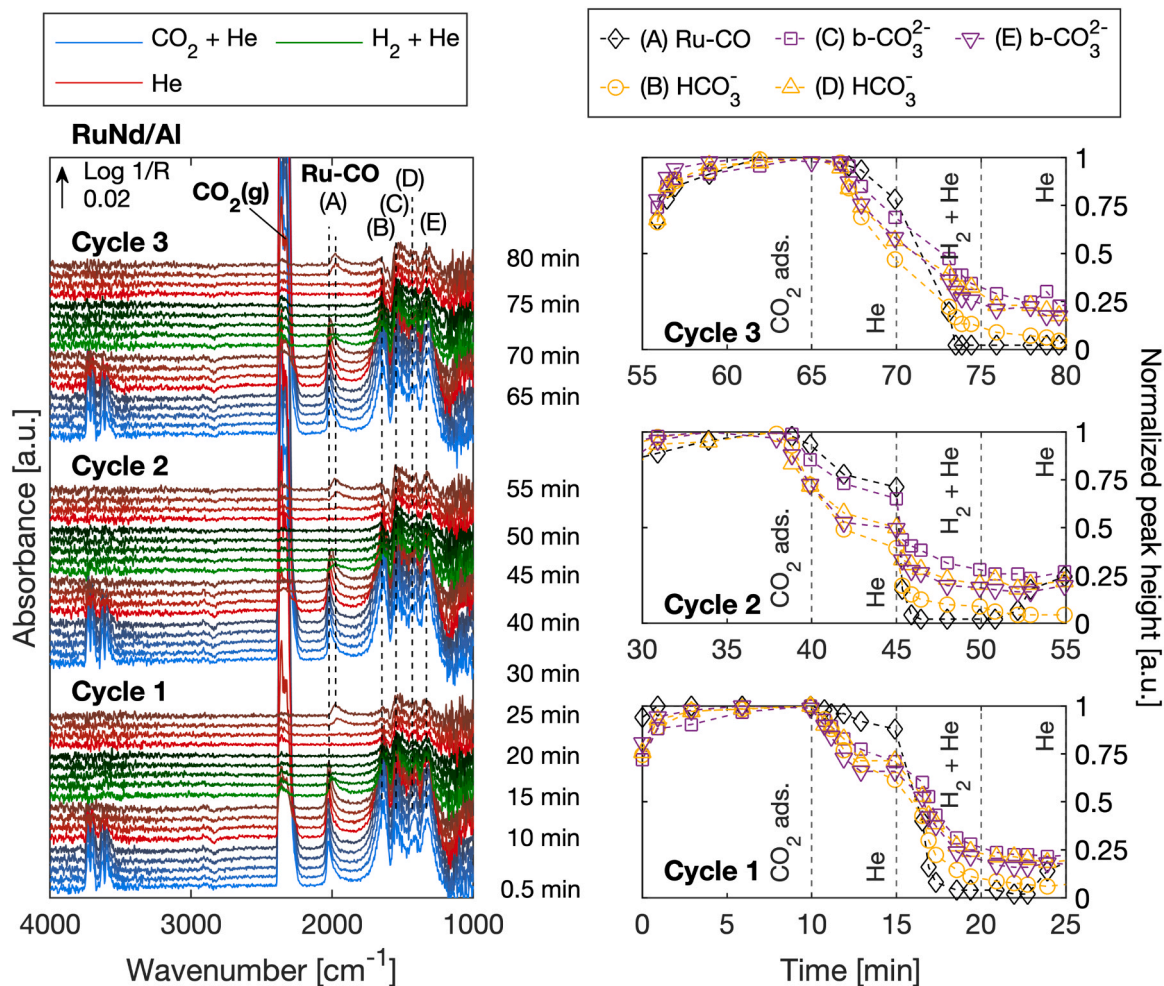


Fig. 11. (left) DRIFTS spectra collected during CO₂ adsorption-hydrogenation cycles at 200 °C, (right) normalized peak heights for Ru-CO (2022–1960 cm⁻¹), HCO₃⁻ (1645 and 1440 cm⁻¹) and b-CO₃²⁻ (1545 and 1330 cm⁻¹) as a function of time.

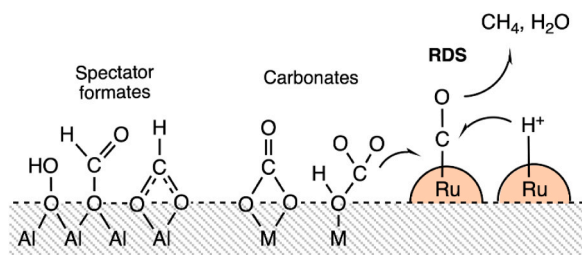


Fig. 12. Simplified reaction pathway for Ru-REO/Al₂O₃ DFMs, showing from left-to-right: formate formation during simultaneous CO₂ and H₂ interaction on the alumina support; CO₂ adsorption as carbonates (bidentate and hydrogen carbonate) adsorption, carbonate surface transport, and the H₂ methanation step (RDS: the rate-determining step). Note: M refers to REO.

or H₂ activation (Fig. 12).

4. Conclusions

This study highlights the significant potential of rare-earth metal oxides (REOs) as adsorbents in ruthenium-alumina-based dual-function materials (DFMs) for CO₂ capture and methanation. Our findings show that incorporating REOs like Gd₂O₃, Sm₂O₃, and Nd₂O₃ into Ru/Al₂O₃ catalysts significantly enhances catalytic performance, particularly at low methanation temperatures (200 °C). The enhanced surface basicity

provided by REOs not only improves CO₂ uptake but also stabilizes the adsorption sites, leading to superior methane production. Specifically, the RuNd/Al catalyst exhibited the highest performance, achieving an 85 % CO₂ capture efficiency and producing methane consistently across 15 cycles, with an average CO₂ uptake of 109 μmol g⁻¹ and methane production of 85 μmol g⁻¹. This represents a CO₂ uptake and methane production increase of +120 % and 30 %, respectively, compared to the unmodified Ru/Al catalyst, which only achieved 49 μmol g⁻¹ CO₂ uptake and 37 μmol g⁻¹ methane production.

Moreover, the addition of REOs improved the stability of carbonates on the catalyst surface during the cycle purges. This stability is crucial as it indicates the potential of REOs in enhancing the durability and reusability of the catalysts over repeated cycles, ensuring consistent performance in long-term applications. This enhancement was clearly demonstrated by the superior performance of the Ru-REO/Al materials in maintaining high CO₂ uptake and methane production over multiple cycles, compared to the degradation observed in non-REO catalysts.

Operando DRIFTS studies provided valuable insights into the surface reactions occurring during CO₂ adsorption and methanation cycles. The presence of carbonates and carbonyl species on the catalyst surface confirmed the adsorption of CO₂ and CO, respectively. The enhanced retention of carbonates observed on Ru-REO/Al catalysts suggested the potential role of REOs in influencing surface reactions and product selectivity.

The results underscore the importance of REOs in improving the stability, efficiency, and selectivity of DFMs, making them highly

effective for CO₂ capture and conversion technologies. The ability of these materials to operate efficiently at lower temperatures not only broadens the operational window but also enhances their applicability in sustainable energy and carbon management strategies. Our study provides a strong foundation for the future development of more efficient and scalable DFMs, with potential applications in industrial CO₂ capture and utilization processes.

CRedit authorship contribution statement

Lizbeth Moreno Bravo: conceptualization, methodology, formal analysis, investigation, data curation, validation, writing – original draft, writing – review and editing. **Frederic C. Meunier:** conceptualization, methodology, writing – original draft, writing – review and editing. **Jan Kopyscinski:** conceptualization, writing – review and editing, supervision.

Declaration of Competing Interest

The authors declare that they have no known competing financial interests or personal relationships that could have appeared to influence the work reported in this paper.

Data Availability

Data will be made available on request.

Acknowledgements

The authors would like to thank CONACYT, Mitacs, and the France-Canada Research Fund for their financial support. Our gratitude extends to IRCELYON for their partnership in this work. Special thanks to the technicians at McGill University who helped with catalyst characterization. David Liu from the FEMR branch for performing TEM-EDS imaging, to Hatem Titi from the Chemistry Department for his aid in optimizing XRD analysis parameters, and to Andrew Golsztajn and Ranjan Roy from the Chemical Engineering Department for their aid with developing the sample digestion method and performing ICP-OES.

Appendix A. Supporting information

Supplementary data associated with this article can be found in the online version at [doi:10.1016/j.apcatb.2024.124591](https://doi.org/10.1016/j.apcatb.2024.124591).

References

- [1] Z. Zhang, S.-Y. Pan, H. Li, J. Cai, A.G. Olabi, E.J. Anthony, V. Manovic, *Renew. Sustain. Energy Rev.* 125 (2020) 109799.
- [2] J. Gao, Q. Liu, F. Gu, B. Liu, Z. Zhong, F. Su, *RSC Adv.* 5 (2015) 22759–22776.
- [3] R. Chauvy, D. Verdonck, L. Dubois, D. Thomas, G. De Weireld, *J. CO₂ Util.* 47 (2021) 101488.
- [4] M.S. Duyar, S. Wang, M.A. Arellano-Treviño, R.J. Farrauto, *J. CO₂ Util.* 15 (2016) 65–71.
- [5] M.A. Arellano-Treviño, Z. He, M.C. Libby, R.J. Farrauto, *J. CO₂ Util.* 31 (2019) 143–151.
- [6] M.S. Duyar, M.A.A. Treviño, R.J. Farrauto, *Appl. Catal. B: Environ.* 168–169 (2015) 370–376.
- [7] I.S. Omodolor, H.O. Otor, J.A. Andonegui, B.J. Allen, A.C. Alba-Rubio, *Ind. Eng. Chem. Res.* 59 (2020) 17612–17631.
- [8] P. Gruene, A.G. Belova, T.M. Yegulalp, R.J. Farrauto, M.J. Castaldi, *Ind. Eng. Chem. Res.* 50 (2011) 4042–4049.
- [9] A. Al-Mamoori, A.A. Rowanghi, F. Rezaei, *ACS Sustain. Chem. Eng.* 6 (2018) 13551–13561.
- [10] J. Ilseemann, M.M. Murshed, T.M. Gesing, J. Kopyscinski, M. Bäumer, *Catalysis Science & Technology* (2020).
- [11] A.S. Farooqi, B.M. Al-Swai, F.H. Binti Ruslan, N.A. Mohd Zabidi, R. Saidur, S. A. Fua'ad Syed Muhammad, B. Abdullah, *IOP Conf. Ser.: Mater. Sci. Eng.* 736 (2020) 042007.
- [12] R.-Y. Chein, W.-Y. Fung, *Int. J. Hydrog. Energy* 44 (2019) 14303–14315.
- [13] A. Bhalkikar, T.-S. Wu, T.J. Fisher, A. Sarella, D. Zhang, Y. Gao, Y.-L. Soo, C. L. Cheung, *Nano Res* 13 (2020) 2384–2392.
- [14] L. Eyring, 1979, L. Eyring, in: *Handbook on the Physics and Chemistry of Rare Earths*, 1979, pp. 337–399.
- [15] D. Li, L. Zeng, X. Li, X. Wang, H. Ma, S. Assabumrungrat, J. Gong, *Appl. Catal. B: Environ.* 176–177 (2015) 532–541.
- [16] G. Zhang, Y. Wang, X. Li, Y. Bai, L. Zheng, L. Wu, X. Han, *Ind. Eng. Chem. Res.* 57 (2018) 17076–17085.
- [17] F. Namvar, M. Salavati-Niasari, F. Meshkani, *Int. J. Hydrog. Energy* 48 (2023) 1877–1891.
- [18] H. Takano, K. Izumiya, N. Kumagai, K. Hashimoto, *Appl. Surf. Sci.* 257 (2011) 8171–8176.
- [19] Q. Pan, J. Peng, T. Sun, D. Gao, S. Wang, S. Wang, *Fuel Process. Technol.* 123 (2014) 166–171.
- [20] Z. Yang, Y. Cui, P. Ge, M. Chen, L. Xu, *Catalysts* 11 (2021) 463.
- [21] A. Bermejo-López, B. Pereda-Ayo, J.A. Onrubia-Calvo, J.A. González-Marcos, J. R. González-Velasco, *J. Environ. Chem. Eng.* 10 (2022) 107951.
- [22] C. Jeong-Potter, A. Porta, R. Matarrese, C.G. Visconti, L. Lietti, R. Farrauto, *Appl. Catal. B: Environ.* 310 (2022) 121294.
- [23] L.-P. Merikouri, T. Ramirez Reina, M.S. Duyar, *Nanoscale* 14 (2022) 12620–12637.
- [24] E. Miyazaki, *J. Catal.* 94 (1980) 84–94.
- [25] J.H. Kwak, L. Kovarik, J. Szanyi, *ACS Catal.* 3 (2013) 2449–2455.
- [26] E. Truszkiewicz, K. Zegadło, D. Wojda, B. Mierzwa, L. Kepiński, *Top. Catal.* 60 (2017) 1299–1305.
- [27] S. Navarro-Jaén, J.C. Navarro, L.F. Bobadilla, M.A. Centeno, O.H. Laguna, J. A. Odriozola, *Appl. Surf. Sci.* 483 (2019) 750–761.
- [28] A. Quindimil, U. De-La-Torre, B. Pereda-Ayo, A. Davó-Quinonero, E. Bailón-García, D. Lozano-Castelló, J.A. González-Marcos, A. Bueno-López, J.R. González-Velasco, *Catal. Today* 356 (2020) 419–432.
- [29] A. Porta, R. Matarrese, C.G. Visconti, L. Castoldi, L. Lietti, *Ind. Eng. Chem. Res.* 60 (2021) 6706–6718.
- [30] M.S. Duyar, A. Ramachandran, C. Wang, R.J. Farrauto, *J. CO₂ Util.* 12 (2015) 27–33.
- [31] L. Falbo, C.G. Visconti, L. Lietti, J. Szanyi, *Appl. Catal. B: Environ.* 256 (2019) 117791.
- [32] C. Jeong-Potter, R. Farrauto, *Appl. Catal. B: Environ.* 282 (2021) 119416.
- [33] E. García-Bordejé, A.B. Dongil, J. Moral, J.M. Conesa, A. Guerrero-Ruiz, I. Rodríguez-Ramos, *J. CO₂ Util.* 68 (2023) 102370.
- [34] L. Proaño, E. Tello, M.A. Arellano-Treviño, S. Wang, R.J. Farrauto, M. Cobo, *Appl. Surf. Sci.* 479 (2019) 25–30.
- [35] L. Österlund, *SSP* 162 (2010) 203–219.
- [36] E.-M. Köck, M. Kogler, T. Bielez, B. Klötzer, S. Penner, *J. Phys. Chem. C* 117 (2013) 17666–17673.
- [37] X. Wang, Y. Hong, H. Shi, J. Szanyi, *J. Catal.* 343 (2016) 185–195.